



Research Article


Adhesion, mobility and aggregation of nanoclusters at surfaces: Ni and Ag on Si, HOPG and graphene



Sergio D'Addato^{1,2,3}  · Federica Perricone¹ · Guido Paolicelli²

Received: 8 September 2021 / Accepted: 11 January 2022

Published online: 31 January 2022

© The Author(s) 2022  OPEN

Abstract

An experimental investigation of Ag and Ni nanoparticles (NPs) deposited on Silicon with its native oxide, on highly oriented pyrolytic graphite and on graphene flakes is reported. The NPs were physically synthesized with a magnetron based gas aggregation source and the produced beam was mass-filtered and deposited in vacuum on the substrates. The study was concentrated on the morphology for the different cases, shedding some light on the interaction of pre-formed NPs with surfaces, a crucial aspect both of technological and scientific relevance. The nature of adhesion can be strongly influenced by the *intrinsic* properties of the surface (like for instance the energetics of interaction between the NP surface atoms and the first layers of the substrate) and/or the *extrinsic* properties, like the presence of defects, step edges, impurities and other irregularities. After adhesion, the NPs mobility and their mutual interaction are very relevant. In this work, the study was concentrated on NP/surface morphology, by using atomic force microscopy, scanning electron microscopy, transmission electron microscopy and X-ray photoelectron spectroscopy.

Article highlights

- Morphology of physically synthesized metal Nano-Particles (NPs) on Si, HOPG and Graphene was investigated. The NPs were pure Ag and Ni.
- Coalescence, diffusion and self-aggregation and preferential adhesion were observed, with possible applications in sensor technology.
- Possible explanations are: NP softness, NP/surface bonding interaction and presence of contaminant species molecules between NP.

Keywords Ni · Ag · Nanoparticles · SEM · AFM · Nanoparticle morphology

Supplementary Information The online version contains supplementary material available at <https://doi.org/10.1007/s42452-022-04944-x>.

✉ Sergio D'Addato, sergio.daddato@unimore.it | ¹Dipartimento FIM, Università di Modena e Reggio Emilia, via G. Campi 213/a, 41125 Modena, Italy. ²CNR-Istituto Nanoscienze, via G. Campi 213/a, 41125 Modena, Italy. ³En&Tech, Università di Modena e Reggio Emilia, via G. Campi 213/a, 41125 Modena, Italy.



SN Applied Sciences

(2022) 4:65

| <https://doi.org/10.1007/s42452-022-04944-x>

1 Introduction

Synthesis and manipulation of metal nanoparticles (NPs) is a research subject of tremendous impact in nanotechnology [1–4]. The bottom-up techniques for NP production includes the vast area of chemical synthesis [5], of self-assembling at surfaces [6], and of physical vapor deposition (PVD) techniques, like Molecular Beam Epitaxy (MBE) [7], pulsed laser ablation [8] and magnetron sputtering followed by gas aggregation [3, 4, 9–11]. In all these cases, interaction of NP with surfaces is a crucial aspect, both of technological and scientific relevance [12–15]. The impact energy of the NP beam on the substrate can alter significantly its shape [13, 15, 16]. In some cases, these changes can be exploited in order to produce new film architecture and morphology [16]. On the other hand, in the so-called soft landing regime, the NP is almost unperturbed, but new relevant phenomena can occur: the nature of adhesion can be strongly influenced by the *intrinsic* properties of the surface (like for instance the energetics of interaction between the NP surface atoms and the first layers of the substrate) [17–19] and/or the *extrinsic* properties, like the presence of defects, step edges, impurities and other irregularities [20–22]. After adhesion, one has to keep into account the NP mobility and their mutual interaction. These relevant and fascinating phenomena have been studied in the past. Bardotti et al. [17] demonstrated experimentally that large Sb clusters could diffuse and self-aggregate on Highly Oriented Pyrolytic Graphite (HOPG) surface. First, they observed that clusters of an average diameter $\langle d \rangle = 5$ nm gave rise to *ramified* islands, an aggregation mode that was a clear proof of diffusion of Sb NPs on such a surface. Second, they simulated with the Montecarlo method the interaction of Sb NPs on the surface, by assuming that it occurs in three different steps: landing, diffusion and aggregation, and they found an excellent agreement with the experiment. Yoon et al. [20] discussed the influence of the cluster size on the type of aggregation of Sb NPs into compact or ramified islands. Generally, the formation of islands takes place after formation of a nucleation center. The other clusters nearby can diffuse and collide successively with the nucleation center within an average time interval Δt . The two competing island morphologies (compact vs. ramified) are determined by Δt and the characteristic time τ necessary for a single cluster to be completely adsorbed into a compact island (coalescence). When $\tau < \Delta t$, the island will retain a compact shape, but beyond a certain value t_0 the clusters will not have enough time to be completely adsorbed, and ramified shapes will start to develop [20]. As mentioned above, irregularities on the substrate (defects, step edges and dislocations) can influence significantly the cluster aggregation [22]. Experiments on Ag clusters deposited on bent HOPG have shown also the effect of surface curvature as a guide to diffusion and

aggregation into islands [21]. Moreover, since these irregularities can act as a guide to the island formation, it is possible to image them with Scanning Electron Microscopy (SEM) by using the clusters as “markers” [22]. In fact, SEM cannot directly image step edges, grains boundaries, grains orientation or elastic strain fields on HOPG bare surfaces [22]. Interestingly, formation of ramified islands have been observed also in experiments of deposition of very small titanium oxide clusters on Au(111) surface [23], showing that this phenomenon is of general relevance. Finally, it was demonstrated that the cluster impact energy and the surface material can give rise to different degrees of adhesion, so it is possible to create areas where the islands density is significantly different [24, 25], with potential applications in the development of new sensors and electronic devices. Surprisingly, these classes of experiments have never been performed on Ni nanoclusters. Ni NPs have peculiar magnetic properties and also have been demonstrated as good candidates in replacing expensive materials (like, for instance Pt) as catalysts [26]. Moreover, the Ni NPs have been extensively studied for the possibility of using them as magnetic memory units, with the use of antiferromagnetic shells to exploit the exchange bias effect and to overcome the superparamagnetic limit [27, 28]. On the other hand, Ag NPs and nanostructures show the surface plasmon resonance, which can be used for instance when coupled with oxides, to enhance visible light absorption, with applications in photo-catalysis and photovoltaics [29, 30].

In this work, the results of a study of deposition of Ni and Ag NPs on carbonaceous (HOPG, Graphene) and Si with its native oxide (Si-SiO_x), are presented. The study was concentrated on NP/surface morphology, by using Atomic Force Microscopy (AFM), SEM, Transmission Electron Microscopy (TEM) and X-ray Photoelectron Spectroscopy (XPS).

2 Experimental

The experimental setup used in this work was described in detail elsewhere [31]. Ni and Ag NP beams were generated using a magnetron based gas aggregation source (OAR NC200U) and mass filtered with an electric quadrupole (QMF). Ar was used as sputtering and aggregation gas. Typical gas flow values varied between $f = 15$ and $f = 60$ sccm. The discharge power was $P = 90$ W for Ni and $P = 35$ W for Ag. After mass selection, the NPs were deposited on a freshly exfoliated HOPG crystal, on a Si wafer with its native oxide (Si-SiO_x) and on graphene (G) flakes obtained by exfoliation and deposited on Si-SiO_x wafers. Si-SiO_x wafers were washed with ethanol before inserting them in the chamber. The deposition rate was measured with a quartz microbalance, and it varied between 0.1 and 1 nm/min for Ni, and between 0.1 and 0.2 nm/min for Ag. In this work the amount of deposited NPs is obtained from

an estimate of the equivalent of a continuous film thickness, given by the measurement of the deposition rate with quartz microbalance, and from a measurement of fractional coverage in the SEM images. The substrates and the NP films were checked in situ with X-ray Photoelectron Spectroscopy (XPS), with a SPECS XR50 twin anode X-ray source, using Mg and Al Ka X-rays and a SPECS PHOIBOS 150 hemispherical electron energy analyzer. The produced samples were successively analyzed with AFM (NDT NTEGRA AURA and VEECO Nanoscope-enviroscope 4 systems) working in tapping mode. SEM images were taken with a Dual beam system (FEI Strata DB235M). The SEM

column is equipped with a Schottky field-emission gun, achieving a resolution of 2 nm. Ag NPs were also imaged with TEM using a JEOL 2200 Fx working at 200 keV and equipped with a Schottky field emission gun (SFEG) with a point-to-point resolution of 0.19 nm.

3 Results and discussion

Figure 1a shows a SEM image of Ni NP deposited on Si-SiO_x, with a fractional coverage C = 7%, corresponding to an estimated thickness of t = 0.3 nm as measured by

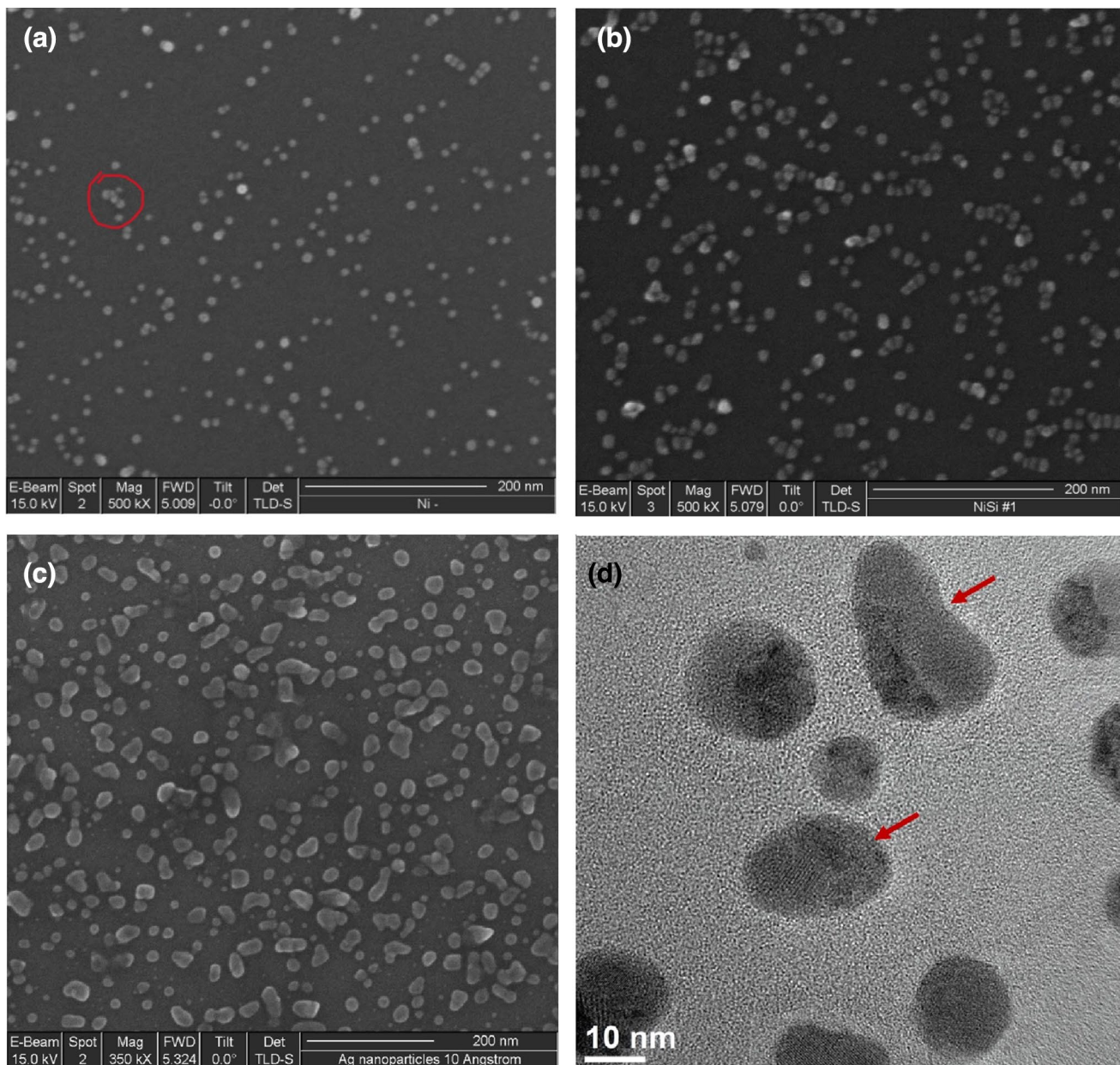


Fig. 1 **a** SEM image of Ni NPs deposited on Si-SiO_x. Fractional coverage C = 7%. **b** same as **(a)**, with C = 14%. **c** SEM image of Ag NPs deposited on Si-SiO_x, C = 30%. **d** TEM image of Ag NPs, showing agglomerates, as indicated by red arrows

quartz microbalance. The NPs are generally dispersed casually on the surface, according to the random paving growth mode, which was already observed on similar systems [13, 14]. Occasionally, some NPs are aggregated (see the area surrounded by a red circle in Fig. 1), probably because they landed on close surface sites. It is interesting to observe that, although the edges are very close, there is still a small gap between two aggregated NPs, i.e. they maintain their individuality. The same behavior can be observed also in the SEM image reported in Fig. 1b, where $C = 14\%$ and $t = 0.6$ nm. In the case of Ag NPs deposited on Si-SiO_x, the situation is very different. The NPs tend to coalesce or to coagulate, they lose their individuality and form agglomerate particles (see Fig. 1b, where Ag NPs assembly has a fractional coverage $C = 30\%$, $t = 1$ nm as measured by quartz microbalance, and also refs. [32]). This phenomenon has been previously observed by an investigation [20] of Sb NPs of an average diameter $d = 5$ nm deposited on (1000) oriented HOPG, as discussed in the introduction.

The TEM image shown in Fig. 1d puts into evidence that the Ag agglomerates are obtained from agglomeration of spherical multitwinned particles, with a consequent polycrystalline shape.

The individual Ag NPs show also deviation from spherical shape. In Fig. 2a SEM and an AFM image from the same sample (Ag NPs on Si-SiO_x) are reported, together with two histograms of lateral size and height distributions, respectively.

The lateral size distribution of Ag NPs is quite broad, with an average diameter $\langle d \rangle = 9.9$ nm, as obtained by fitting the distribution with a lognormal function, and a Full Width Half Maximum $Dd = 6$ nm. The height distribution shows instead two distinct structures, peaked at $h_1 = 2.8$ nm and $h_2 = 5.9$ nm respectively. This distribution could be fitted with two gaussian profiles, with the following parameters:

$\langle h_1 \rangle = 2.8$ nm, $h_1 = 2$ nm, $\langle h_2 \rangle = 6$ nm, $h_2 = 3$ nm, where Δh is the full width half maximum of the Gaussian profiles. The first peak can be attributed to the Si-SiO_x

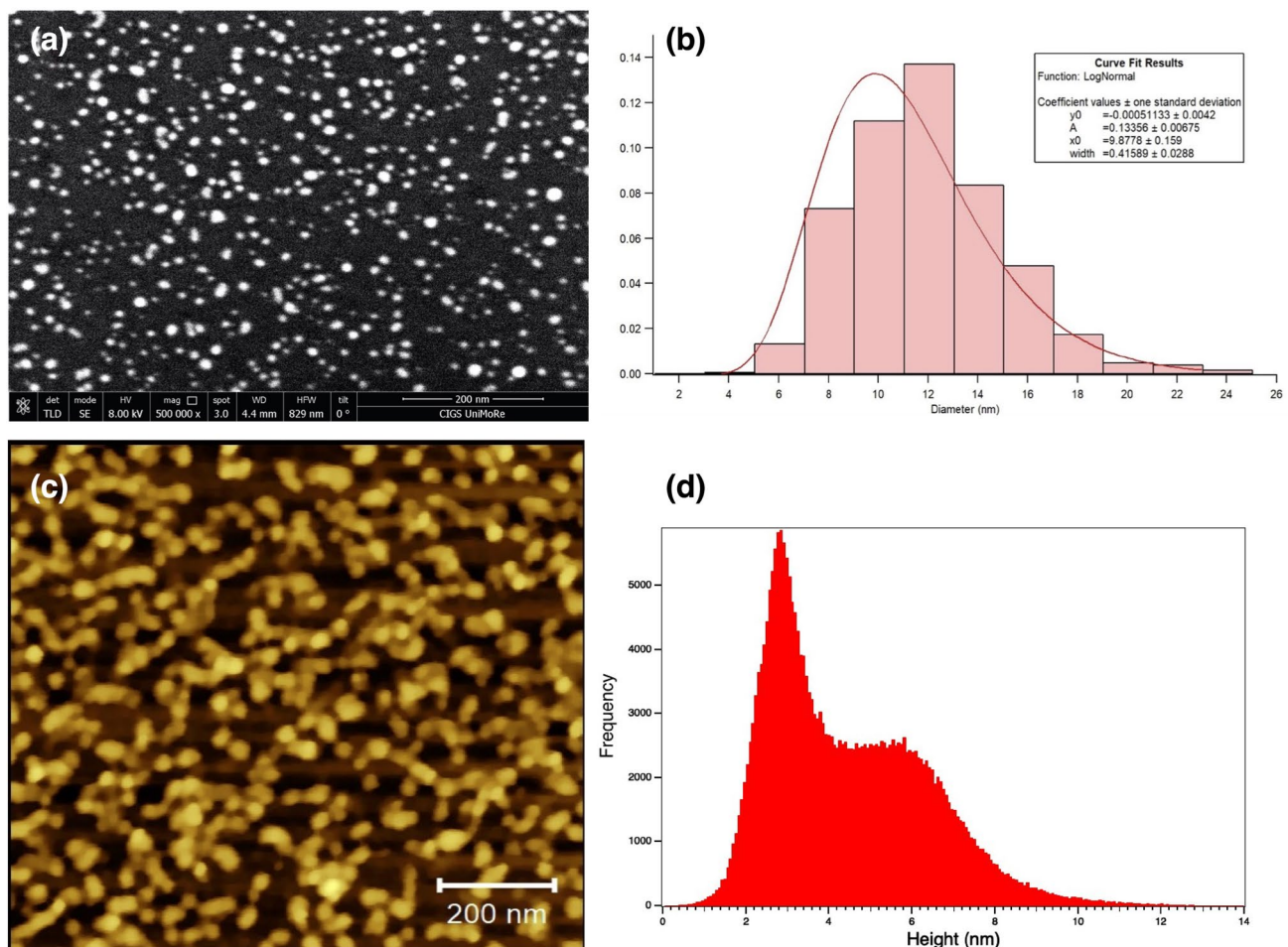


Fig. 2 **a** SEM image of Ag NP deposited on Si-SiO_x. Fractional coverage $C = 14\%$. **b** histogram showing the lateral size distribution as obtained by grain analysis of **(a)**. **c** AFM image from the same sample as **(a)**. **d** Height distribution obtained by the line profile analysis of **(c)**

substrate height distribution, referenced to the height minimum as measured during the line scan, while the second one is due to the NP height distribution. A rough estimate of the average height of the NP can be obtained by subtracting $\langle h_1 \rangle$ from $\langle h_2 \rangle$, obtaining $\langle h \rangle = 3.2$ nm. Thus, the Aspect Ratio (AR) of the NPs can be obtained by performing the division $AR_{Ag} = \langle d \rangle / \langle h \rangle = 3.0$. From this analysis, we obtain that there is a significant NP flattening. As previously reported [32], this effect has two causes: deviation of NPs from the original shape after landing, because of interaction with the substrate, and the

presence of coalesced NPs caused by diffusion and aggregation [18–20]. In a previous [19] and in the present study on Ni NPs deposited on Si-SiO_x using the same growth parameters it was found out $\langle d_{Ni} \rangle = 5.5$ nm, $\langle h_{Ni} \rangle = 4$ nm, with $AR_{Ni} = 1.4$. The different behavior of the two types of NPs can be ascribed to a higher number of agglomerates and possibly to a lower stiffness of Ag with respect to Ni, which favors a more substantial change of shape of the former with respect to the latter.

A very different situation occurs when Ni NP are deposited on HOPG. In this case, the morphology drastically

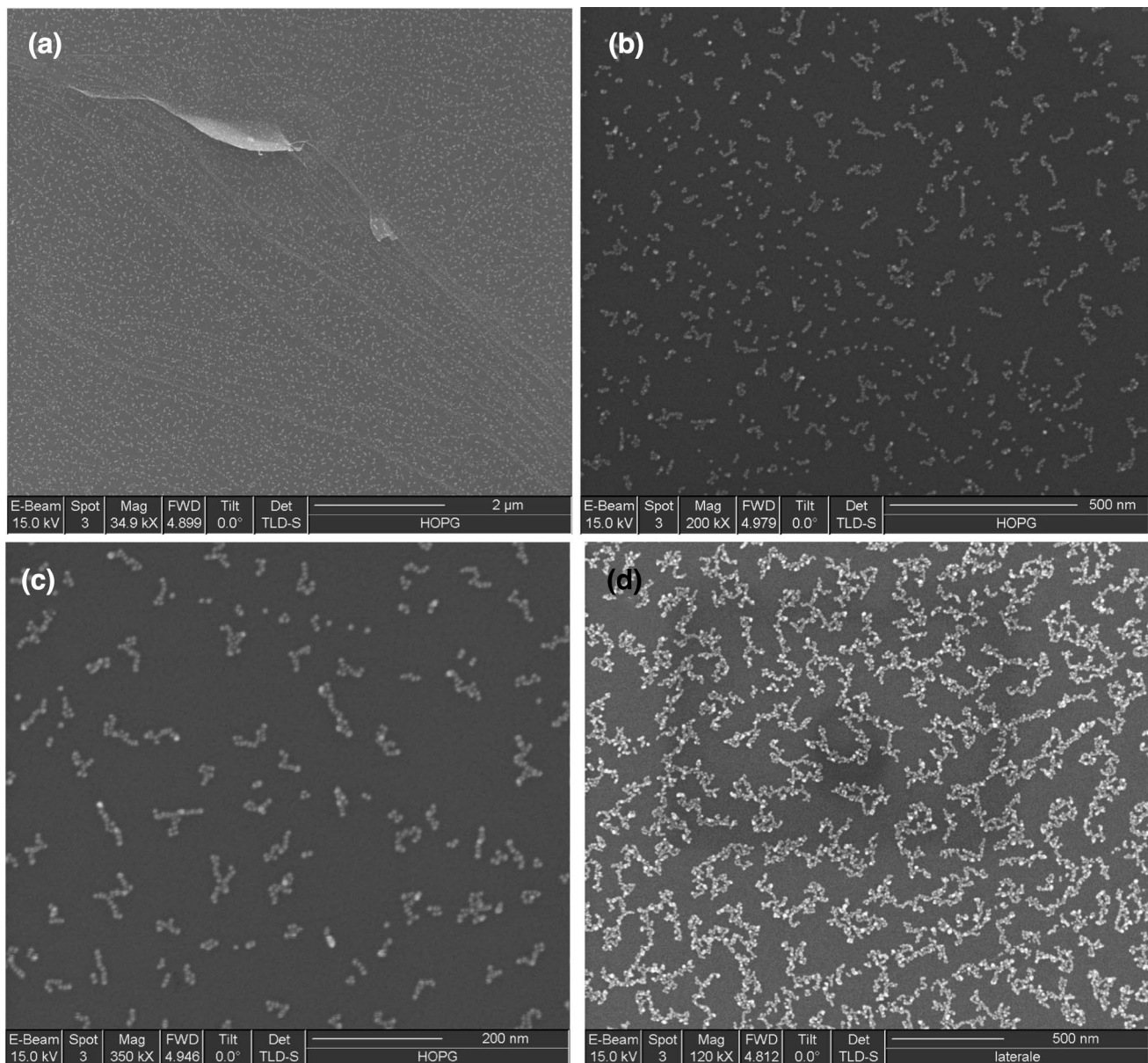


Fig. 3 **a** SEM image taken from Ni NP deposited on HOPG with a fractional coverage $C = 4\%$ of NP on the surface. The image magnification was $M = 34.9$ kX. **b** same as **(a)** taken from the same sample,

with $M = 200$ kX. **c** same as **(b)**, with $M = 350$ kX. **d** SEM image taken from a sample with a fractional coverage $C = 15\%$ after annealing in atmosphere at $T = 500$ K for $t = 30$ min, $M = 120$ kX

changes. In Fig. 3a–c SEM images from Ni NPs on HOPG are reported from the same sample, at different magnification values. Looking at Fig. 3a, b, it is evident that we have two different situations: single NPs and small chains decorating the steps obtained by the HOPG exfoliation procedure (see Fig. 3a, b) and formation of aggregates on flat areas. These aggregates show some beginning of ramification, and they are consistent with a high degree of diffusion on the graphite surface, although more limited than for Ag [21, 22] and Sb [17, 20]. At increasing coverage, after annealing at $T=500$ K for 30 min in air, the aggregates extend and form complex ramified structures, with chains of length up to few hundreds of nm. Diffusion is favored by the high temperature, while the mechanism of chain formation is probably due to sequential sticking of the clusters (one after another) and to the energetics of the substrate-NP and NP-NP interaction [20].

The diffusion coefficient D Ni NPs can be roughly estimated following the work by Bardotti et al. [17]. The used formula is

$$D = \left(\frac{0.41}{N_{agg}} \right)^{\frac{1}{\chi}} F \pi d^4 / 16 \quad (1)$$

where N_{agg} is the average number of NP aggregates (or “islands”), as measured by counting the number of aggregates of two or more NPs in the SEM images and normalizing them to the number possible sites of nucleation in the same image (calculated by counting the maximum number of particles of average diameter d that can be arranged in close-packed surface geometry), F is the incident flux of NP on the substrate during deposition, d is the average particle diameter (measured by analyzing the Ni NP SEM images) and $\chi = 0.336$. It was obtained that $N_{agg} \approx 0.0043$ agg/site, and assuming a value $d = 6$ nm for the Ni NP diameter, a value $D \approx 10^{-11} \text{ cm}^2 \text{ s}^{-1}$ was obtained, significantly smaller than the one obtained by Bardotti et al. [17] for Sb NPs ($d = 5$ nm) on HOPG ($D \approx 10^{-8} \text{ cm}^2 \text{ s}^{-1}$). The cause of this significant discrepancy is uncertain; it can be possibly ascribed to a different substrate for the two experiments, and to a much higher degree of adhesion of Ni NPs to the surface with respect to Sb, due to the faceting of Ni NPs which have a multitwinned structure [11].

Another difference with respect to Ag is that Ni does not form continuous islands, i.e. there is a distance between the surface two adjacent NPs even in the aggregates.

A possible cause for this difference can be a higher stiffness of Ni NP, preventing coalescence, but it could be due either to residual contaminant gas species in the vacuum system or to species adsorbed on the HOPG surface. Figure 4a show the XPS spectrum of the HOPG substrate and of the Ni NP/HOPG sample. The C 1 s, Ni 2p and C KLL and Ni LVV series are clearly visible and do not show differences

from clean HOPG and bulk Ni spectra. In Fig. 4b the Ni 2p core level spectrum shows a metal-like lineshape, as previously observed [31]. Nevertheless, a careful inspection revealed presence of traces of O before and after deposition, as shown in Fig. 4c, probably due to contamination after the peeling procedure in atmosphere and during NP deposition. Unfortunately, it was not possible in our system to heat the substrate prior the NP deposition to remove contaminant species. The O 1 s signal intensity normalized to C 1 s increased from 0.1 to 0.6% after the dosing of NP. In the case of deposition on Si-SiO_x, the spectra show a higher degree of O and C contamination before Ni deposition, as it can be seen from Fig. 4a, because the Si wafer was not atomically cleaned. Nevertheless, from Fig. 4c, the Ni 2p core level spectra after deposition does not show any sign of changes with respect to the one obtained from Ni NP/HOPG. A similar situation occurred for Ag NP deposition on Si-SiO_x. The Ag 3d XPS spectrum from NP on this substrate is reported on Fig. 4d. Again, the spectrum is very similar to the ones obtained from clean Ag films and surfaces [6].

The effect of contaminants on the morphology was discussed for Au and Pt NP on carbon films [33]. Depending on the base vacuum in the experimental system, it was found that the NP could form ramified islands or could self-organize in aggregates of hexagonal geometry. In particular, it was found that the distance between the edges of two adjacent Pt NP had an average value $d_{edge} = 1.2 \pm 0.2$ nm, and it was inferred that this distance was caused by adsorption of CO molecules sticking out of the Pt NP surface [33]. Similar results were recently obtaining on Au nanoclusters, where the letting in of small quantity of water lead to the formation of small (2 or 3) aggregates separated by H₂O molecules, as confirmed also in molecular dynamics simulations [34]. In our case, the limited resolution of the used SEM did not allow to measure the edge-edge distance of Ni NPs with the necessary accuracy. In previous works it was found that a shell of defective NiO was obtained after exposure to oxygen [30]. It is possible that some oxidation of the NPs surface occurred during their deposition, giving rise to the NP passivation of their first atomic layer and to a distancing between the NP edges. Figure 3d reports a SEM image of Ni NPs on HOPG after annealing in atmosphere at $T = 500$ K. The high temperature favors the diffusion of NP and formation of greater aggregates with ramification and chains, as a further demonstration that NPs can diffuse to a great extent on HOPG surfaces. It is interesting also to note that many aggregates have linear sizes of hundreds of nm. The complex morphology is obtained probably by diffusion, either of single NP or small aggregates, and attachment to bigger complexes, as also found in previous experiments [17, 21, 22].

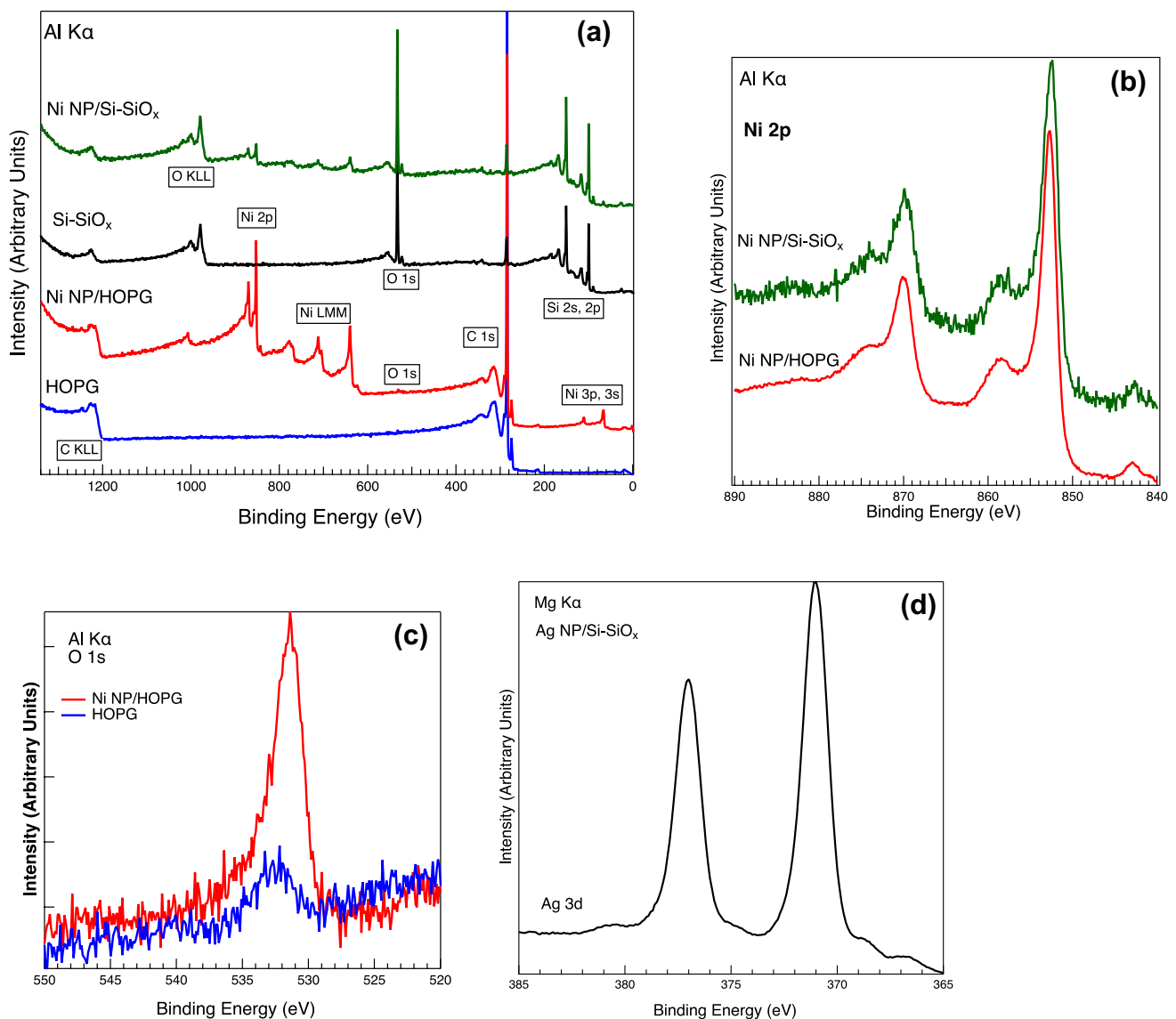


Fig. 4 **a** XPS spectra of HOPG, Si-SiO_x prior and after deposition of Ni NPs in the extended region. The major features appearing in the spectra are labeled. **b** Ni 2p core levels spectra from Ni NPs, showing the typical metal-like features distinctive of clean Ni. The two spectra are normalized to their maxima. **c** O 1s core level spectra prior and after deposition of NPs on HOPG, showing and increas-

ing in oxygen amount, although the signal intensity is less than 1% with respect to C 1s. **d** Ag 3d spectrum from Ag NP deposited on Si-SiO_x. Spectra reported on figures (a) to (c) were obtained using Al Kα photons ($h\nu = 1486.7$ eV), while spectrum on (d) was obtained with Mg Kα photons ($h\nu = 1253.6$ eV)

The type of substrate has an influence not only on the NP diffusion and aggregation, but also on the NP adhesion to the surface. The sticking probability of NPs can vary drastically for heterogeneous surfaces made of areas with different materials, as it was reported for Bi, Sb and Cu nanoclusters [25]. Also, it can depend on NP kinetic energy before the impact and on the incident geometry [35]. The SEM images shown in Fig. 5 are a confirmation of this phenomenon also for Ni NPs.

In this case, G flakes obtained by exfoliation were deposited on Si-SiO_x surface. The sample was then

exposed to the Ni NP beam generated by the nanocluster source and investigated with SEM. The area density of NPs on G flakes is much higher than on bare Si-SiO_x surface. The cause of this behavior can be a more effective bonding between the C electron p states in G and the Ni electron d states on the NP surface. It was previously reported with HR-TEM analysis that the Ni NP show a multi-twinning icosahedral structure, exposing (111) facets [31]. On the other hand, it was also demonstrated that G layers are absorbed more effectively (stronger bonding) on the (111) surface on Ni with respect to other transition metals, because

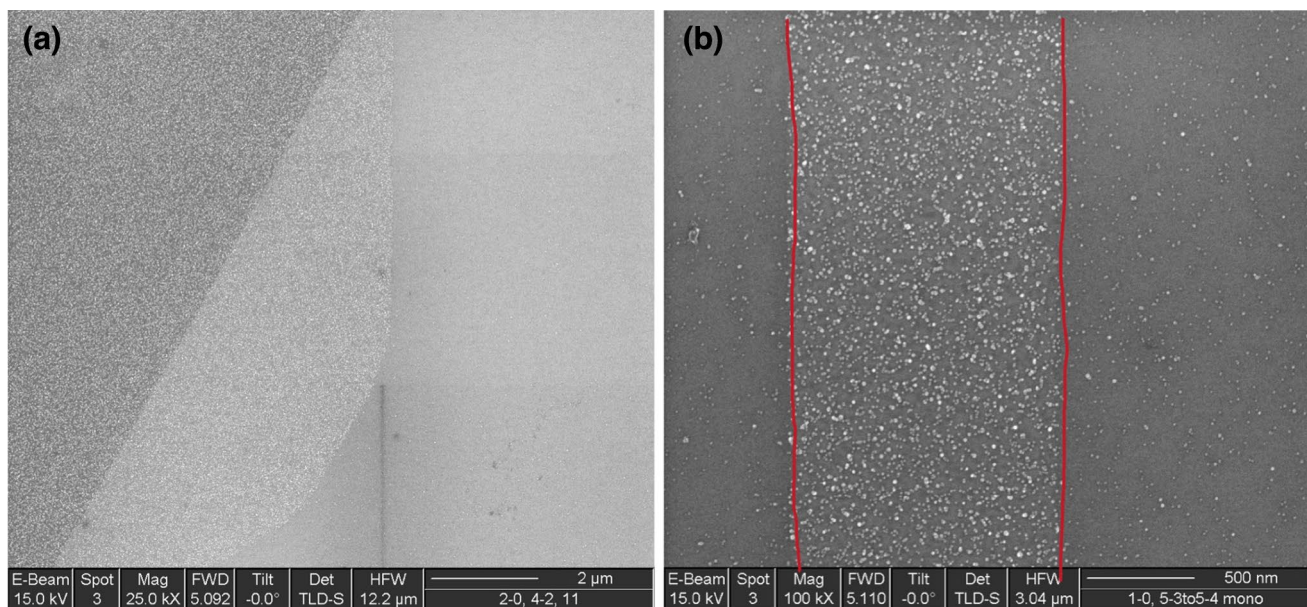


Fig. 5 SEM image of Ni NPs on G flakes deposited on Si-SiO_x. **a** 2-layer (darker area on top-left), 1-layer G (stripe in the center area) and bare Si surface (right) after Ni deposition. **b** Stripe -shaped G

flake and bare Si surface, showing that the Ni NP assembly is much denser on G. The red lines put in evidence the borders between the flake and the bare surface

of the good lattice matching, (see for instance ref. [36]). In this specific case, the situation is somehow specular: Ni(111) facets interacts with pre-formed G layer, instead of C atoms absorption on Ni(111), but the nature and strength of the two interfaces should be very similar. On the contrary, the adhesion of Ni NP on Si-SiO_x should be less favored, because of the passivation of the Si-SiO_x after exposure to the atmosphere. The differential adhesion of NPs on heterogeneous surfaces can be of potential interest in nanoelectronics and nano-sensor technology [24, 25]. The resulting morphologies and behavior of Ag and Ni NPs deposited on the four different surfaces are summarized in Table 1.

4 Conclusions

We reported an experimental investigation of the morphology of physically synthesized Ag and Ni NP adsorbed on Si-SiO_x, HOPG and G flakes by making use of SEM and AFM. A significant aspect ratio (AR = 3) was found for Ag NPs on Si, mainly due to limited diffusion,

coalescence of single NPs and to interaction with the substrate. This behavior is not observed in the case of Ni. Although some small aggregates are present, coalescence is not present, and the NPs preserve their individuality. Also there is no evidence of diffusion on large scale on Si-SiO_x. When Ni NPs are deposited on HOPG, formation of greater aggregates is observed, caused by diffusion of NP and self-organization in ramified structures. Single NPs also tend to decorate steps and act as nucleation centers for the island formation. After heating the substrates to T = 500 K, the aggregates grow in size and complexity, as diffusion is more pronounced. Even in the islands, Ni NPs do not coalesce, at variance with Ag NPs, and they maintain their individuality, similarly to other NPs. A possible explanation is the presence of residual gas species on the substrate and in deposition chamber blocking NPs direct bonding. At present, this assertion is only qualitative, and more experiments are needed, assisted by theoretical calculations, although there are similar cases in the literature. Finally, it was also observed that for Ni NPs, when deposited on heterogeneous G/Si surface, there is preferential adhesion

Table 1 Behavior of Ag and NP assemblies on Si-SiO_x, HOPG and graphene flakes deposited on Si-SiO_x

Ag NP/Si-SiO _x	Ni NP/Si-SiO _x	Ni NP/HOPG	Ni NP/G/Si-SiO _x
Coalescence, sintering, deviation from original spherical shape	Agglomerates without sintering, random paving	Diffusion on flat areas and beginning of formation of ramified islands, single NP decorating HOPG steps	Random paving, preferential adhesion to G flakes

to G-covered areas, with potential interesting consequences in nano-sensor technology and electronics.

Acknowledgements We thank Vincenzo Grillo for the TEM measurements and Christian Alvino for the G/Si-SiO_x sample preparation.

Data availability Available under request. Please contact the corresponding author.

Code availability Commercial licensed software was used for data treatment and analysis.

Declarations

Conflict of interest There are no conflicting/competing interests in this work.

Open Access This article is licensed under a Creative Commons Attribution 4.0 International License, which permits use, sharing, adaptation, distribution and reproduction in any medium or format, as long as you give appropriate credit to the original author(s) and the source, provide a link to the Creative Commons licence, and indicate if changes were made. The images or other third party material in this article are included in the article's Creative Commons licence, unless indicated otherwise in a credit line to the material. If material is not included in the article's Creative Commons licence and your intended use is not permitted by statutory regulation or exceeds the permitted use, you will need to obtain permission directly from the copyright holder. To view a copy of this licence, visit <http://creativecommons.org/licenses/by/4.0/>.

References

- Schmidt G (2004) Nanoparticles. Wiley-VCH, Weinheim
- Johnston RL (2012) Metal nanoparticles and alloys. *Front Nanosci* 3:1–42. <https://doi.org/10.1016/B978-0-08-096357-0.00006-6>
- Huttel Y (2017) Gas-phase synthesis of nanoparticles. Wiley-VCH, Weinheim
- D'Addato S, Spadaro MC (2018) Low pressure bottom-up synthesis of metal@oxide and oxide nanoparticles: control of structure and functional properties (invited comment). *Phys Scr* 93:033001. <https://doi.org/10.1088/1402-4896/aa9db7>
- Sun SH, Murray CB, Weller D, Folks L, Moser A (2000) Monodisperse FePt nanoparticles and ferromagnetic FePt nanocrystal superlattices. *Science* 287:1989–1992. <https://doi.org/10.1126/science.287.5460.1989>
- D'Addato S, Gunnella R, Borgatti F, Felici R, Finetti P (2007) Atom geometry of nanostructured Fe films grown on c(2x2)-N/Cu(100) surface: an investigation by X-ray absorption spectroscopy with multishell analysis. *Surf Sci* 601:329–340. <https://doi.org/10.1016/j.susc.2006.09.036>
- Luches P, Pagliuca F, Valeri S, Illas F, Preda G, Pacchioni G (2012) Nature of Ag islands and nanoparticles on the CeO₂(111) surface. *J Phys Chem C* 116:1122–1132. <https://doi.org/10.1021/jp210241c>
- Wegner K, Piseri P, Tafreshi HV, Milani P (2006) Cluster beam deposition: a tool for nanoscale science and technology. *J Phys D Appl Phys* 39:R439–R452. <https://doi.org/10.1088/0022-3727/39/22/R02>

9. Haberland H, Karrais M, Mall M (1991) A new type of cluster and cluster ion source. *Z Phys At Mol Clust* 20:413–415. <https://doi.org/10.1007/BF01544025>
10. Martínez L, Mayoral A, Espiñeira M, Roman E, Palomares FJ, Huttel Y (2017) Core-shell Au@TiO_x nanoparticles by gas-phase synthesis. *Nanoscale* 9:6463–6473. <https://doi.org/10.1039/C7NR01148B>
11. D'Addato S, Grillo V, di Bona A, Luches P, Frabboni S, Valeri S, Lupo P, Casoli F, Albertini F (2013) Controlled co-deposition of FePt nanoparticles embedded in MgO: a detailed investigation of structure and electronic and magnetic properties. *Nanotechnology* 24:495703. <https://doi.org/10.1088/0957-4484/24/49/495703>
12. Jensen P (1999) Growth of nanostructures by cluster deposition: experiments and simple models. *Rev Mod Phys* 71:1695–1735. <https://doi.org/10.1103/revmodphys.71.1695>
13. Binns C (2001) Nanoclusters deposited on surfaces. *Surf Sci Rep* 44:1–49
14. Binns C, Trohidou KN, Bansmann J, Baker SH, Blackman JA, Bucher J-P, Kechrakos D, Kleibert A, Louch S, Meiwes-Broer K-H, Pastor GM, Perez A, Xie Y (2005) The behaviour of nanostructured magnetic materials produced by depositing gas-phase nanoparticles. *J Phys D Appl Phys* 38:R357–R379. <https://doi.org/10.1088/0022-3727/38/22/R01>
15. Haberland H, Karrais M, Mall M, Thurner Y (1992) Thin films from energetic cluster impact: a feasibility study. *J Vac Sci Technol A* 10:3266–3271. <https://doi.org/10.1116/1.577853>
16. Haberland H, Insepov Z, Moseler M (1995) Molecular-dynamics simulations of thin-film growth by energetic cluster impact. *Phys Rev B* 51:11061–11067. <https://doi.org/10.1103/PhysRevB.51.11061>
17. Bardotti L, Jensen P, Hoareau A, Treilleux M, Cabaud B (1995) Experimental observation of fast diffusion of large antimony clusters on graphite surfaces. *Phys Rev Lett* 74:4694–4697. <https://doi.org/10.1103/PhysRevLett.74.4694>
18. Kleibert A, Bulut F, Gebhardt RK, Rosellen W, Sudfeld D, Passig J, Bansmann J, Meiwes-Broer KH, Getzlaff M (2008) Correlation and shape anisotropy of supported mass-filtered Fe and FeCo alloy nanoparticles on W(110). *J Phys Condens Matter* 20:445005. <https://doi.org/10.1088/0953-8984/20/44/445005>
19. D'Addato S, Gagnaniello L, Valeri S, Rota A, di Bona A, Spizzo F, Panozaqi T, Schifano SF (2010) Morphology and magnetic properties of size-selected Ni nanoparticle films. *J Appl Phys* 107:104318. <https://doi.org/10.1063/1.3374467>
20. Yoon B, Akulin VM, Cahuzac Ph, Carlier F, de Frutos M, Masson A, Mory C, Colliex C, Bréchnignac C (1999) Morphology control of the supported islands grown from soft-landed clusters. *Surf Sci* 443:76–88. [https://doi.org/10.1016/S0039-6028\(99\)00988-7](https://doi.org/10.1016/S0039-6028(99)00988-7)
21. Schmidt M, Kébaïli N, Lando A, Brezzak S, Baraton L, Cahuzac Ph, Masson A, Bréchnignac C (2008) Bent graphite surfaces as guides for cluster diffusion and anisotropic growth. *Phys Rev B* 77:205420. <https://doi.org/10.1103/PhysRevB.77.205420>
22. Kébaïli N, Benrezzak S, Cahuzac P, Masson A, Bréchnignac C (2009) Diffusion of silver nanoparticles on carbonaceous materials. Cluster mobility as a probe for surface characterization. *Eur Phys J D* 52:115–118. <https://doi.org/10.1140/epjd/e2009-00067-y>
23. Goodman KR, Wang J, Ma Y, Tong X, Stacchiola DJ, White MJ (2020) Morphology and reactivity of size-selected oxide nanoclusters on Au(111). *J Chem Phys* 152:054714. <https://doi.org/10.1063/1.5134453>
24. Partridge JG, Brown SA, Dubar ADF, Reiche R, Kaufmann M, Siegert C, Scott S, Blaikie RJ (2004) Templated-assembly of conducting antimony cluster wires. *Nanotechnology* 15:1382–1387. <https://doi.org/10.1088/0957-4484/15/9/045>
25. Reichelt R, Partridge JG, Natali F, Matthewson T, Brown SA, Lassesson A, Mackenzie DMA, Ayesh AI, Tee KC, Awasthi A, Hendy SC (2006) From the adhesion of atomic clusters to the fabrication of nanodevices. *Appl Phys Lett* 89:213105. <https://doi.org/10.1063/1.2387894>
26. Xie L, Kirk DW (2020) Stability comparison of Pt and Ni as base metal catalysts in anion exchange membrane fuel cells. *J Electrochem Soc* 167:064519. <https://doi.org/10.1149/1945-7111/ab8368>
27. Skumryev V, Stoyanov S, Zhang Y, Hadjipanayis G, Givord D, Nogués J (2003) Beating the superparamagnetic limit with exchange bias. *Nature* 423:850. <https://doi.org/10.1038/nature01687>
28. Ponti A, Ferretti AM, Capetti E, Spadaro MC, Bertoni G, Grillo V, Luches P, Valeri S, D'Addato S (2017) Steering the magnetic properties of Ni/NiO/CoO core-shell nanoparticle films: the role of core-shell interface vs interparticle interactions. *Phys Rev Mat* 1:036001. <https://doi.org/10.1103/PhysRevMaterials.1.036001>
29. Catchpole KR, Polman A (2008) Design principles for particle plasmon enhanced solar cells. *Appl Phys Lett* 93:191113. <https://doi.org/10.1063/1.3021072>
30. Pelli Cresi JS, Principi E, Spurio E, Catone D, O'Keeffe P, Turchini S, Benedetti S, Vikatakavi A, D'Addato S, Mincigrucci R, Foglia L, Kurdi K, Nikolov IP, De Ninno G, Masciovecchio C, Nannarone S, Kesavan JK, Boscherini F, Luches P (2021) Ultrafast dynamics of plasmon-mediated charge transfer in Ag@CeO₂ studied by free electron laser time-resolved X-ray absorption spectroscopy. *Nano Lett.* 21:1729. <https://doi.org/10.1021/acs.nanolett.0c04547>
31. D'Addato S, Grillo V, Altieri S, Tondi R, Valeri S, Frabboni S (2011) Structure and stability of nickel-nickel oxide core-shell nanoparticles. *J Phys Condens Matter* 23:175003. <https://doi.org/10.1088/0953/23/17/175003>
32. D'Addato S, Pinotti D, Spadaro MC, Paolicelli G, Grillo V, Valeri S, Pasquali L, Bergamini L, Corni S (2015) Influence of size, shape and core-shell interface on surface plasmon resonance in Ag and Ag@MgO nanoparticle films deposited on Si/SiO_x. *Beilstein J Nanotechnol* 6:404–413. <https://doi.org/10.3762/bjnano.6.40>
33. Bardotti L, Tournus F, Mélinon P, Pellarin M, Broyer M (2011) Self organization of Pt and Au clusters deposited on graphite: the role of reactivity. *Eur Phys J D* 63:221–224. <https://doi.org/10.1140/epjd/e2011-10579-4>
34. Zhao J, Mayoral A, Martinez L, Johansson MP, Djukarebova F, Huttel Y (2020) Core-satellite gold nanoparticle complexes grown by inert gas-phase condensation. *J Chem Phys C* 124:24441–24450. <https://doi.org/10.1021/acs.jpcc.0c07346>
35. Ayesh AI, Brown SA, Awasthi A, Hendy SC, Convers PY, Nichols K (2010) Coefficient of restitution for bouncing nanoparticles. *Phys Rev B* 81:195422. <https://doi.org/10.1103/PhysRevB.81.195422>
36. Grünels A, Vyalikh DV (2008) Tunable hybridization between electronic states of graphene and a metal surface. *Phys Rev B* 77:193401. <https://doi.org/10.1103/PhysRevB.77.193401>

Publisher's Note Springer Nature remains neutral with regard to jurisdictional claims in published maps and institutional affiliations.